ARTICLE

L-Tyrosine on Ag(111): Universality of the Amino Acid 2D Zwitterionic Bonding Scheme?

Joachim Reichert,[§,⊥] Agustin Schiffrin,[†,‡,*] Willi Auwärter,[⊥] Alexander Weber-Bargioni,[§] Matthias Marschall,[⊥] Martina Dell'Angela,[∥,#] Dean Cvetko,[∥,▽] Gregor Bavdek,[∥,▽] Albano Cossaro,[∥] Alberto Morgante,[∥,#] and Johannes V. Barth[§,⊥]

[†]Department of Chemistry, The University of British Columbia, Vancouver, British Columbia V6T 1Z4, Canada, [‡]Max-Planck-Institut für Quantenoptik (MPQ), Hans-Kopfermann-Strasse 1, D-85748 Garching, Germany, [§]Department of Physics & Astronomy, The University of British Columbia, Vancouver, British Columbia V6T 1Z4, Canada, [⊥]Physik Department E20, Technische Universität München, James Franck Strasse, D-85748 Garching, Germany, [∥]C.N.R.-INFM, Laboratorio Nazionale TASC, Trieste, Italy, [#]Dipartimento di Fisica, Universita di Trieste, Trieste, Italy, and [▽]Physics Department, University of Ljubljana, Jadranska 19, SI-1000, Ljubljana, Slovenia

ABSTRACT We present a combined study of the adsorption and ordering of the L-tyrosine amino acid on the close-packed Ag(111) noble-metal surface in ultrahigh vacuum by means of low-temperature scanning tunneling microscopy (STM), X-ray photoelectron spectroscopy (XPS) and near-edge X-ray absorption fine structure (NEXAFS) spectroscopy. On this substrate the biomolecules self-assemble at temperatures exceeding 320 K into linear structures primarily following specific crystallographic directions and evolve with larger molecular coverage into two-dimensional nanoribbons which are commensurate with the underlying atomic lattice. Our high resolution topographical STM data reveal noncovalent molecular dimerization within the highly ordered one-dimensional nanostructures, which recalls the geometrical pattern already seen in the L-methionine/Ag(111) system and supports a universal bonding scheme for amino acids on smooth and unreactive metal surfaces. The molecules desorb for temperatures above 350 K, indicating a relatively weak interaction between the molecules and the substrate. XPS measurements reveal a zwitterionic adsorption, whereas NEXAFS experiments show a tilted adsorption configuration of the phenol moiety. This enables the interdigitation between aromatic side chains of adjacent molecules *via* parallel-displaced $\pi-\pi$ interactions which, together with the hydrogen-bonding capability of the hydroxyl functionality, presumably mediates the emergence of the self-assembled supramolecular nanoribbons.

KEYWORDS: amino acids · supramolecular self-assembly · scanning tunneling microscopy · noble-metal surfaces · X-ray photoelectron spectroscopy · X-ray absorption spectroscopy

*Address correspondence to agustin.schiffrin@mpq.mpg.de.

Received for review November 22, 2009 and accepted January 12, 2010.

Published online January 21, 2010. 10.1021/nn901669p

When tracked down to their most minimal form, the specific structural order and inherent functionality of living organisms appear as the consequence of well-defined processes taking place at the nanoscale.[1] Among these elementary mechanisms that drive the behavior of complex biological systems one can distinguish the relevance of noncovalent supramolecular interactions, which are accountable for crucial biochemical procedures such as molecular self-assembly, self-recognition, and geometric conformation,[2,3] to name a few. Therefore, a better fundamental understanding of order phenomena at the molecular level can provide insight in the global characterization of more complex biologically relevant systems. In the particular case of polypeptides for example, the stability or denaturation of the specific secondary and tertiary structure of proteins are mediated by noncovalent interactions such as hydrogen-bonding[4] or aromatic−aromatic interactions[5−8] between the side chains of the amino acid units.

Now, the molecular-level examination of low-dimensional biomolecular assemblies on well-defined surfaces can yield such elementary portrayal. Furthermore, the control of these assembly processes defines a promising approach for the design of one-dimensional (1D)[9−12] and two-dimensional (2D)[13−15] functional nanostructures by employing the inherent functionality and specific noncovalent bonding capacity of the molecular building units. The choice of a supporting substrate is crucial for the determination of the state for such nanostructures given that the structural symmetry and chemical properties of the underlying lattice can have dramatic effects on the conformational and chemical states of the adsorbed molecular systems.[16−19] Thus, such bioinspired procedure for a controlled nanostructuring and functionalization of surfaces advances the paradigm of bottom-up design to overcome the limitations dictated by current top-down nanofabrication techniques and explore novel pathways toward low-dimensional materials.

Because of this fundamental biological relevance of noncovalent intramolecular interactions and their potential for low-

dimensional noncovalent synthesis at the nanoscale, the study of such supramolecular binding schemes on surfaces has become a major field of research in nanoscience.[20−22] Now, when it comes to probe the real-space morphology of low-dimensional nanostructures, scanning tunneling microscopy (STM) and spectroscopy (STS) represent a powerful analytical tool with which it becomes possible to locally describe the interactions between biomolecules in a perfectly controlled environment. By the means of these methods, the self-assembly of amino acids and other organic molecules on metallic surfaces has been studied, along with the chemical, electronic, and morphological effects on the system induced by the substrate properties.[11,23−29] Whereas it is not always straightforward to derive with STM and STS the chemical and electronic properties of the observed nanosystems, this often becomes possible when these real-space techniques are coupled to complementary spectroscopic methods such as X-ray photoemission and absorption spectroscopies, allowing a complete physicochemical characterization at the nanoscale.

In this work we present a low-temperature STM study and characterization of the self-assembly of the L-tyrosine amino acid (COOH−CH(NH_2)−CH_2−C_6H_4−OH, see Figure 1*a* for a structure model) on the close-packed noble-metal surface Ag(111) under ultrahigh vacuum (UHV) conditions. The interest in studying the behavior of single amino acids on metal surfaces resides in their inherent potentiality as functional building nanounits, but also in the fact that this approach might yield further fundamental insight in the role of specific amino acids composing more complex peptide chains with a given biological relevance. In the particular case of L-tyrosine for instance, it is suspected to be involved in metal−ligand interactions which might alter the biological function of specific peptides.[30] Morphological studies of amino acid adsorption (L-tyrosine included) on metal surfaces have already been performed in the past,[24,29,31,32] as well as their chemical considerations in solid-state thin films.[33−38] A related noteworthy example of amino acid self-assembly on a noble-metal surface is given by L-methionine (COOH−CH(NH_2)−CH_2−CH_2−S-CH_3) on Ag(111), which has been considered in our previous work.[32] This system is characterized by regular nanogratings composed of linear biomolecular nanowires consisting in parallel zwitterionic amino acid dimers which are adjacently linked by hydrogen bonds. On highly ordered pyrolytic graphite the adsorption of this amino acid shows an identical self-assembly morphology.[39] Here, by considering the case of L-tyrosine on Ag(111), we address the influence of the amino acid side chain on the equilibrium configuration of the supramolecular assembly. A combined morphological and chemical study of the case of L-tyrosine on the weakly reactive Ag(111) surface in UHV conditions has not been undertaken so far. On

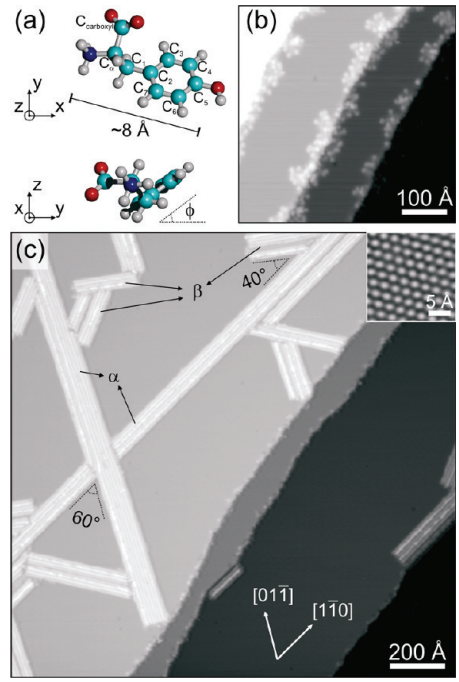

Figure 1. Constant-current STM topographs of L-tyrosine on Ag(111). (a) Structure model of the L-tyrosine amino acid zwitterion seen from different directions. We define ϕ as the angle between the adsorption plane of the molecule and the phenol side chain plane. Color code for molecular model: cyan is carbon, red is oxygen, blue is nitrogen, white is hydrogen. Carbon atoms are labeled. (b) Amino acid molecules deposited at 170 K: molecules diffuse and form clusters decorating the substrate step edges (I = 0.1 nA, V = 500 mV). (c) Deposition at 170 K and then annealed at 320 K: supramolecular self-assembled domains extend under the influence of the underlying substrate symmetry (I = 0.1 nA, V = 500 mV). Inset: atomic resolution image of the Ag(111) substrate.

this surface the biomolecules self-assemble at 320 K into linear structures primarily following specific crystallographic directions. Our high-resolution topographical STM data reveals molecular dimerization within the highly ordered 1D nanostructures, which recalls the geometrical pattern already seen for L-methionine on Ag(111),[32] on Cu(111),[40] and for cysteine on Au(110).[24] This supports a universal noncovalent self-assembling scheme for amino acids on weakly reactive smooth metal surfaces. With increasing molecular coverage the biomolecular nanowires evolve into wider 2D sheet-structured domains which are commensurate with the underlying atomic lattice and whose formation is associated with the reactivity of the amino acid phenol residue. Complementary X-ray photoelectron spectroscopy (XPS) and near-edge X-ray absorption fine structure (NEXAFS) experiments were carried out in order to obtain information on the system regarding its chemical state and molecular conformation. Whereas XPS evidence a zwitterionic adsorption, the NEXAFS measurements show a tilted adsorption of the *L*-tyrosine phenol ring with respect to the substrate plane, allowing interdigitation and parallel-displaced π−π stacking between the side chains of adjacent mol-

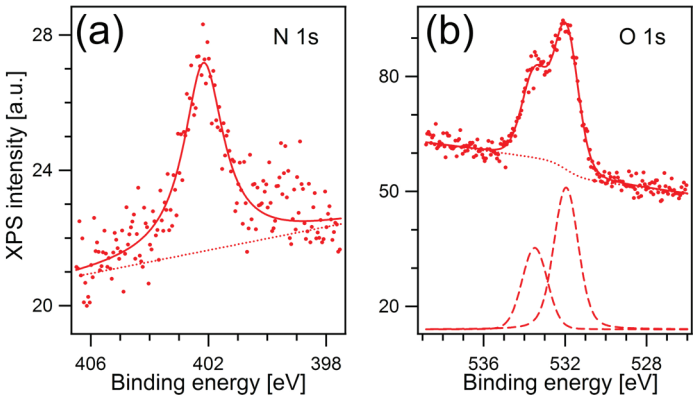

Figure 2. XPS data of L-tyrosine on Ag(111) in the N 1s and O 1s core level regions for the high temperature submonolayer phase. (a) N 1s data points are fitted (solid line) with a Shirley background (dotted line) and a single Voigt peak centered at a binding energy of 402.2 ± 0.2 eV. This peak is assigned to the ammonium group NH_3^+. (b) O 1s data points are fitted (solid line) with a Shirley background (dotted line) and two Voigt curves (dashed line) positioned at binding energies of 532.0 ± 0.1 and 533.5 ± 0.1 eV. These peaks are assigned to the equivalent resonant oxygen atoms of the carboxylate group and to the oxygen atom of the hydroxyl group respectively.

ecules. This noncovalent hydrogen-bonded network involving the carboxylate, ammonium, and phenol functional groups is reminiscent of the L-tyrosine crystallization in three dimensions (3D).[41] Moreover, the molecules desorb when the system is heated above 350 K indicating that the interacting force between the molecules and the Ag(111) surface is relatively small.

RESULTS AND DISCUSSION

The morphology of the L-tyrosine self-assembly on Ag(111) is illustrated in the topographical STM images in Figure 1b,c. Figure 1a depicts the structure model of the L-tyrosine amino acid. We define here the angle ϕ as the angle between the phenol ring and the molecular adsorption plane. When the molecules are deposited onto the Ag(111) surface held at 170 K the molecules diffuse to the step edges where they are pinned. However, the molecules gather in clusters and show no particular ordering pattern (Figure 1b). The STM image in Figure 1c illustrates the same sample preparation as in Figure 1b, following annealing at a temperature of 320 K for 5 min. Here we observe the emergence of ordered supramolecular ribbons. These features show a bias-independent apparent height of 2.0 ± 0.2 Å. The thermally induced molecular rearrangement observed from Figure 1b to Figure 1c implies that a certain activation barrier has to be overcome to form the linear ordering of the supramolecular arrays. The inset represents an atomic resolution image of the underlying Ag(111) substrate, allowing the determination of the growth orientations of the linear biomolecular self-assembly with respect to the Ag(111) atomic lattice. The supramolecular architectures can be separated in two different groups α and β, α being composed of biomolecular entities following the ⟨110⟩ crystalline orientations of the substrate, whereas the structures β follow a $-40 \pm 2°$ (i.e., clockwise) tilt with respect to the α component. These preferred orientations of the molecular growth evidence the influence of the substrate symmetry and geometry on the self-assembly. However, the substrate−molecule interaction seems not stringent, as reflected by the fact that the nanostructures can be easily manipulated in their orientation during the STM data acquisition (see Figure S1 in the Supporting Information). This is corroborated by the low molecular desorption temperature, occurring when the system is heated above 350 K.

Moreover, the extension of phase β with a $-40°$ angle and the absence of its mirror-image orientation as a favored direction with respect to the substrate high-symmetry axes, reveals the enantiomorphism of the biomolecular assembly. If the self-assembly was achiral, an equivalent mirror-symmetric structure propagating along a $+40°$ angle with respect to the ⟨110⟩ orientations should be experimentally observed. This non-mirror-symmetric supramolecular configuration on the achiral Ag(111) surface is the expression of the amino acid stereocenter at the α-carbon. The extrapolation of the molecular level chirality into the biomolecular ensemble on an achiral surface has already been observed for L-methionine on Ag(111) and Cu(111),[40] and is the consequence of preferential adsorption sites on the substrate atomic lattice for the amino, carboxyl, and side chain functional groups of the molecule.

The adsorption of L-tyrosine on Cu(111) at a substrate temperature of 290 K has also been considered, showing substrate-induced molecular dissociation. The molecules were deposited onto pristine monocrystalline Cu(111) under the same conditions as on Ag(111), which irrefutably demonstrates that the observed adsorbed entities correspond to submolecular fragments of the amino acid and not to a possible contamination of the surface or decomposition during evaporation. The chemical nature of the molecular fragments was not established, and further spectroscopic studies are required for this purpose. This molecular fragmentation can be explained by a chemical dissociation triggered by the interaction between the amino acid functional groups and the Cu(111) surface, the latter being more reactive than the Ag(111) surface (see Figure S2 in the Supporting Information for more details).

XPS and NEXAFS spectroscopy measurements were performed to resolve the chemical and conformation state of the molecules within the ordered self-assembled biomolecular nanostructures on Ag(111). Figure 2 illustrates the N 1s and O 1s XPS data resolving the chemical state of the amino acid functional groups. These results correspond to the equilibrated sample annealed at 320 K at a submonolayer molecular coverage. Measurements for the low temperature preparation were also carried out, showing no temper-

ature dependence on the system chemical state (see Figure S3 in the Supporting Information for a N 1s XPS data set of the low temperature phase). The NEXAFS spectra also showed no variation with the sample preparation temperature. The fact that the X-ray spectroscopic measurement showed no dependence on the preparation temperature clearly demonstrates that the ordered high temperature phase is not triggered by a thermally induced chemical reaction or conformational change of the molecular geometry, but that it is driven by kinetic equilibration. The XPS N 1s data in Figure 2a were fitted with only one Voigt peak centered at a binding energy of 402.2 ± 0.2 eV. Our previous studies of the L-methionine amino acid adsorbed on Ag(111)[32] and Cu(111)[40] revealed a N 1s XPS signature for a positively charged ammonium group NH_3^+ at binding energies of 401.2 and 401.3 eV, respectively, and at 399.5 eV for a neutral amino group NH_2 in the case of Cu(111).Therefore, we conclude that the N 1s peak at 402.2 ± 0.2 eV in our present case corresponds to an ammonium group. The discrepancy of about 1 eV with respect to the L-methionine/Ag(111) case can be due to an increased distance between the ammonium group and the metal surface, resulting in a reduced screening process of the nitrogen core hole by the substrate conduction electrons. In Figure S3b of the Supporting Information section one can see that a second N 1s XPS peak appears at 399.8 ± 0.5 eV with increasing X-ray exposure time. This second peak is associated with a neutral amino group and evidences an X-ray mediated deprotonation of the ammonium group. This X-ray induced effect on amino acids has been previously observed in work from Zubavichus *et al.*[33] In Figure 2a consequences of the X-ray exposure are already present at ~399.5 eV, but one can undoubtedly claim that only the peak at 402.2 eV corresponds to the signature of the intrinsic chemical state of the system.

On the other hand, the O 1s XPS data in Figure 2b were fitted with two Voigt peaks at binding energies of 532.0 ± 0.1 and 533.5 ± 0.1 eV. These peaks are assigned respectively to the equivalent resonant oxygen atoms of the negatively charged carboxylate group and the side chain hydroxyl group. These binding energy values and such correspondence to the functional groups of the molecule is consistent with the work from Zubavichus *et al.*[33] The ratio between the areas of the peak at 533.5 eV and the peak at 532.0 eV is 0.55, which reflects the 1:2 stoichiometry between the hydroxyl and carboxylate oxygens. According to this interpretation, we deduce a zwitterionic state for the adsorbed species. Again, the carboxylate O 1s binding energy of 532.0 eV shows a significant shift with respect to the value of 531.2 eV found for L-methionine on Ag(111)[32] and the value of 531.5 eV for the L-methionine/Cu(111)[32] case. As aforementioned, this could be due to a slightly different adsorption configuration of the amino acid on the metal substrate given the different side chain, implying a different distance between the surface and the carboxylate group and thus different electronic screening conditions.

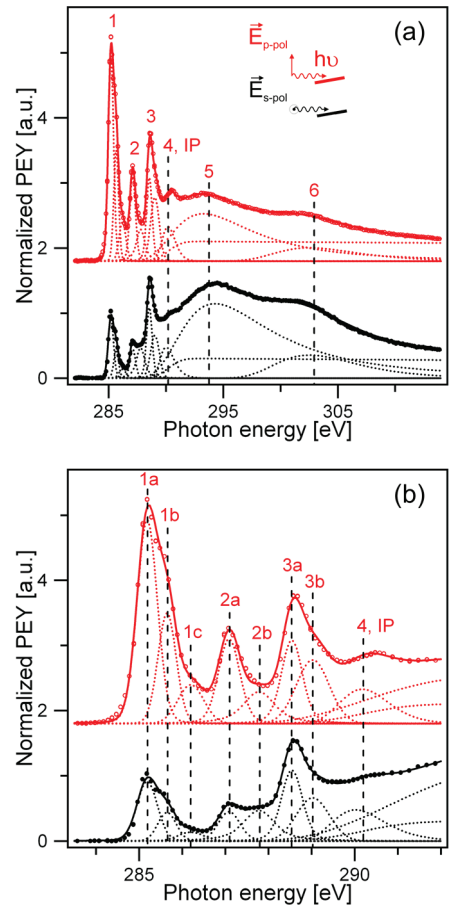

Figure 3. C 1s NEXAFS spectra of the L-tyrosine/Ag(111) system for the saturated monolayer high temperature phase. (a) C 1s absorption edge in p-polarization (red) and s-polarization (black). Markers represent the experimental data, dotted curves the fitting peaks, and the solid line the resulting total fit. Vertical dashed lines indicate the peak positions. Decreased signal intensity of the π* resonances for the s-polarization data reveals a preferred adsorption orientation of the phenol π system. The phenol ring adsorbs in an oblique fashion with respect to the substrate. (b) Detail of the pre-IP zone. The IP edge was modeled with an error function centered at 290.2 eV. Peaks 1a, 1b, 1c, and 2a and curve 3a are related to the phenol and carboxyl π* resonances, respectively. The p-polarization spectrum is offset for clarity.

NEXAFS spectroscopy measurements were performed for the C 1s edge in order to obtain orientational information of the side chain phenol ring with respect to the Ag(111) substrate plane. The high temperature phase spectra for the p- and s-polarization geometries are shown in Figure 3 (red and black, respectively). The partial electron yield (PEY) spectra were fitted according to the building block principle[42] with Voigt peaks, asymmetric Gaussian curves, and a Gaussian-convoluted step function (*i.e.*, error function) positioned at a photon energy of 290.2 eV which takes account of the ionization potential (IP) step. The fitting parameters and assignment for each peak are summa-

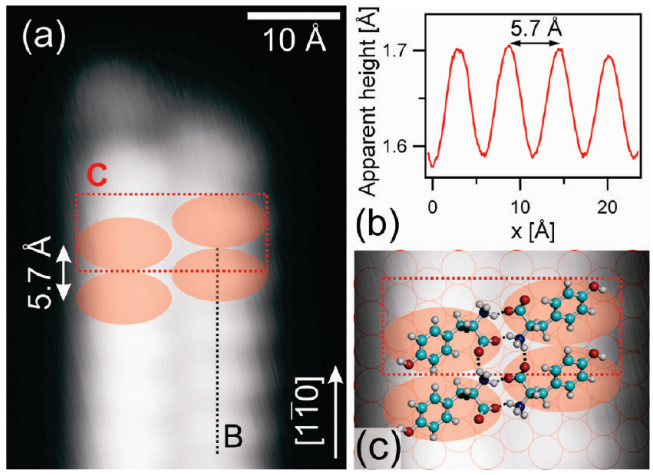

Figure 4. High resolution STM data and molecular model of the submonolayer biomolecular self-assembly of L-tyrosine on Ag(111). (a) Ordered biomolecular chains extending along the [1, −1, 0] crystalline orientation of the Ag(111) substrate appear after annealing the system at 320 K. Molecules dimerize along their long axis and bind adjacently and commensurably with the atomic lattice along the chain direction. The two red ellipses in frame C represent two zwitterions forming a hydrogen-bonded dimer (I = 0.2 nA, V = 500 mV). (b) Apparent height profile along line B. (c) Molecular model of the hydrogen-bonded dimer on the Ag(111) atomic lattice. Hydrogen bonds involving the carboxylate and ammonium groups of the zwitterions are shown as dashed lines.

rized in Table S1 of the Supporting Information section. The assignment of each peak to a given resonance of the chemical features of the adsorbed molecule is performed in accordance with previous experimental and theoretical NEXAFS studies on amino acids or functional groups.[33,36,43,42,44−46]

The features observed in the NEXAFS spectra can be divided in two categories: sharp pre-IP edge peaks related to C 1s → π* resonances (peaks 1a, 1b, 1c, 2a, and 3a in Figure 3b) and broader peaks extending beyond the IP edge associated with C 1s → σ* resonances (peaks 2b, 3b, 4, 5, and 6 in Figure 3b).[42] In particular, the sharp peaks 1a, 1b, 1c, and 2a correspond to π* resonances of the side chain phenol ring (see Table S1 in Supporting Information). The strong dichroism of these features reveals a preferred adsorption angle for the phenol group with respect to the surface: if the adsorbed molecules showed a random internal geometry, both p- and s-polarization signals should average to the same value. As aforementioned, the spectra show no temperature dependence, which is an evidence of the same intramolecular conformational geometry for both phases. We note that the formation of ordered supramolecular domains which follows the temperature annealing does not alter the NEXAFS dichroism, indicating that the orientation of the phenol moiety does not change upon molecular dimerization and emergence of the ordered 1D nanostructures. Added to the temperature independence of the XPS data, this confirms that the thermally activated ordering of the nanoribbons is a consequence of the self-assembly and not of a thermally triggered chemical or conformational change.

Also, the nonvanishing signal of these sharp peaks for the s-polarization indicates a tilted adsorption of the phenol group with respect to the substrate plane. Given the 3-fold symmetry of the substrate and that the π* orbital of the phenol ring is oriented perpendicular to the aromatic plane following an angle δ with respect to the polarized photon electric field ε, the proportionality of the respective NEXAFS signal to $\cos^2(\delta)$ yields for the angle φ between the phenol and the substrate plane:[42]

$$\phi(I_p/I_s) = \arcsin\sqrt{\frac{2\cos^2\theta}{(I_p/I_s) + 3\cos^2\theta - 1}} \qquad (1)$$

where θ is the photon incident angle (here, θ = 7°), and I_p and I_s are respectively the p- and s-polarization NEXAFS intensities related to the phenol π* resonances. In this expression, a perfectly linear polarization of the X-ray beam is assumed. The intensities I_p and I_s are given by the areas of the fitting Voigt and Gaussian functions, and deriving an angle φ for each of the four π* resonances related to the phenol ring, we obtain an average adsorption angle of $\langle\phi\rangle = 37° \pm 3°$. The error bar of this value takes account of the assumption of perfect linear polarization of the incident X-ray radiation, of the error on the angle between polarization vector and sample surface, and of the error of the fitting procedure. This oblique adsorption geometry of the aromatic moiety is consistent with density functional theory calculations performed on the phenylalanine amino acid on noble-metal surfaces, which demonstrated an adsorption with the substrate *via* the nitrogen and carboxyl oxygen atoms and where the π-conjugated system was not involved in the binding to the metal.[47]

Details on the molecular structural arrangement within the ordered biomolecular arrays on Ag(111) are displayed in Figure 4 and Figure 5. We focus here on the linear nanowires and 2D nanoribbons composing structure α of the high temperature phase, that is, the one expanding along the ⟨110⟩ orientations of the substrate. Figure 4a displays a STM image of a biomolecular chain which self-assembled with the substrate held at 240 K. The 1D structure is composed of identically shaped elliptical units, each of which we assign, due to geometrical arguments, to a single L-tyrosine zwitterion. Within these 1D chains, the amino acid molecules appear always in pairs with the 1D extension given by parallel dimers bound adjacently: no ordered nanostructure with an odd number of molecules has been observed in the system. A similar molecular dimerization and adjacent bonding pattern has been already revealed in the self-assembly of the L-methionine amino acid on Ag(111)[32] and Cu(111).[40] Along the linear extension orientation, the L-tyrosine chain shows a molecular periodicity of 5.7 ± 0.1 Å (Figure 4b), showing commensurability of the structure in this direction, as this value

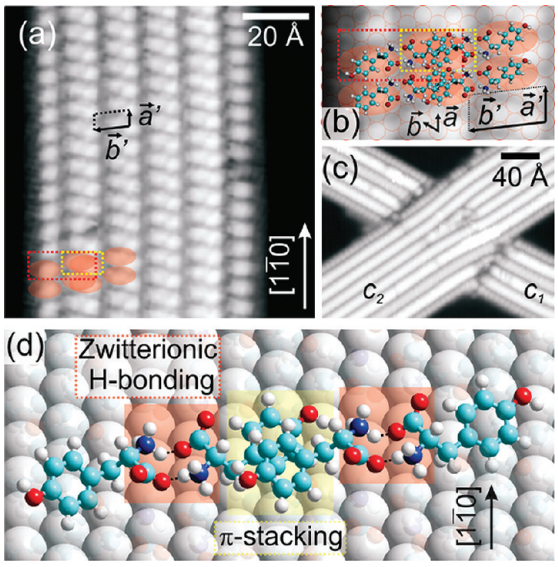

Figure 5. Emergence of 2D L-tyrosine supramolecular nanoribbons on Ag(111). (a) STM data of wider commensurately ordered supramolecular ribbons appearing after annealing at 320 K (I = 0.07 nA, V = 500 mV). (b) Molecular model of the supramolecular arrangement within a self-assembled nanoribbon. The red rectangle frames the hydrogen-bonded dimer within a simple row, whereas the yellow one represents two molecules of adjacent rows with their π-stacked phenol side chains. Linear extension of the self-assembly along the close-packed crystalline axes is given by adjacent hydrogen-bonding between parallel molecules. (c) Chain merging and intercrossing give hints of the molecular self-assembly dynamics: wider ribbons are preferred due to a higher number of π interactions between phenol groups and therefore to a thermodynamically more favorable configuration with lower total energy (I = 0.1 nA, V = 500 mV). (d) Schematic of the intermolecular bonding mechanism within the wider amino acid nanostructure: the zwitterion dimerizes *via* head-to-head hydrogen bonds between carboxylate and ammonium groups (red rectangle), and wider commensurate supramolecular sheets result from merging of simple bimolecular chains *via* parallel-displaced π−π interactions between the phenol side chains (yellow rectangle).

corresponds to twice the Ag(111) lattice constant along the close-packed orientations ⟨110⟩ ($a_{Ag(111)}$ = 2.89 Å). The STM data suggest that within a supramolecular chain two molecules dimerize with their long axis collinear with each other. In this configuration, the molecules can either bind in a head-to-head fashion, with their carboxylate and ammonium groups facing each other, or in a tail-to-tail scheme, with the hydroxyl groups binding together. As in our previous studies,[32,40] we performed MM+ force-field simulations[48,49] to estimate the intermolecular interactions between two L-tyrosine zwitterions confined in 2D in antiparallel and parallel configurations (see Figure S4 in the Supporting Information for the interacting energy maps of a two-molecule system in these dispositions). For the antiparallel case, these calculations result in an optimal head-to-head dimerization with an interaction energy on the order of −1.5 eV per molecular dimer, and where the negatively charged carboxylate group faces the positively charged ammonium residue (see Figure S4a in the Supporting Information). The long-range 1D extension is then given by adjacently bound parallel dimers, which is supported by the MM+ calculations for the parallel two-molecule system (see Figure S4b in the Supporting Information). Our model proposed in Figure 4c for the noncovalent supramolecular arrangement within the 1D nanowires takes account of these energetically favorable considerations. Although it is true that this force-field approach is inefficient to accurately evaluate hydrogen bonding and π interactions,[50] it has at least the potential to point out at the electrostatic character of the interactions involving the electronegative hydroxyl group and the partially charged carboxylate and ammonium groups. It is important to note that this bonding scheme is essentially identical to the one of L-methionine on the same surface[32] and on Cu(111),[40] and might represent a general bonding trend for amino acids adsorbed on metal surfaces in their zwitterionic state.

A key difference between the L-methionine and L-tyrosine self-assemblies resides in the nonformation of regular nanogratings in the latter. In fact, we observe the appearance of wider molecular domains after annealing the system at 320 K (Figure 5a). This can be explained by the increased chemical reactivity of the amino acid phenol side chain. From geometrical arguments the emergence of these ribbons must imply the merging and partial overlapping of narrower supramolecular rows, with intercalation of the phenol moieties. This can be perceived in Figure 5a,b where molecular dimers (framed in red) intercalate (yellow frame marks the interdigitation region) in order to match a commensurate adsorption with the underlying atomic lattice. In fact, the periodicity and commensurability of the molecular arrangement within these wider domains can be seen in Figure 5b, where the supramolecular unit cell is defined by the vectors **a**′ and **b**′. Considering the periodic atomic lattice of the Ag(111) substrate and its unit cell given by vectors **a** and **b**, one can explicitly associate the supramolecular and substrate periodicities, and write **a**′ = 2**a** and **b**′ = −3**a** + 5**b**. The intercalation of merged narrower rows is possible due to the tilted adsorption of the phenol ring shown by the NEXAFS spectroscopic data, which enables parallel-displaced π−π stacking between parallel aromatic residues. Such π−π interactions have been theoretically evaluated to be in the range of −0.12 to −0.16 eV[51−55] for a dimer of aromatic rings, which, even if they remain lower than electrostatic interactions and strong hydrogen bonding, have been proven to compete with the latter for driving low-dimensional supramolecular self-assemblies.[56] Moreover, it has been demonstrated that such interactions play a critical role in terms of protein stabilization[5−8] and in more general structural properties of biological systems at the molecular level.[57] The intermolecular bonding scheme within these interdigitated supramolecular nanoribbons is thus summarized

in the 3D schematic in Figure 5d and consists in the synergy of head-to-head zwitterionic hydrogen-bonding given by the general amino acid functionality, with the L-tyrosine specific side chain intercalation mediated by parallel-displaced $\pi-\pi$ stacking. This is reminiscent of the noncovalent ordering pattern in 3D L-tyrosine crystals.[41] Furthermore, this linear self-assembly scenario recalls the case of diphenyl oxalic amide on Au(111), where an oblique adsorption of the π-conjugated system is a prerequisite for hydrogen-bonding between parallel adjacent molecules.[58,59] The main difference is that in our present study the distance between interdigitated aromatic planes is on the order of 3 Å and hence within the range of parallel-displaced $\pi-\pi$ stacking, mediating the emergence of commensurate 2D sheet nanostructures. [51]

The STM data in Figure 5c reveals the complexity of the self-assembly process. Here, a biomolecular domain c_1 is segmented by a wider domain c_2. The fact that both segments of c_1 present the same width, orientation, and intradomain imaging contrast is a strong indication that these sections were part of the same initial structure, and that the segmentation is directly due to the merging of c_1 with the wider structure c_2. Given that within our model the wider chain-structured sheets are realized *via* attractive $\pi-\pi$ interactions between neighboring aromatic rings with tilted geometry, one would expect the occurrence of larger ribbons to be thermodynamically favorable and therefore predominant with respect to smaller ones. Indeed, we observe in the spatial intersection between extended ribbons in Figure 5c that the wider domain (c_2) shows better stability than the narrower one (c_1).

CONCLUSION

Our high-resolution low-temperature STM observations show the anisotropic self-assembly of the L-tyrosine amino acid on Ag(111). Our data reveal the influence of the substrate symmetry on the morphology of the biomolecular nanostructures and the molecular organization pattern within the supramolecular domains. Complementary space-averaging XPS and NEXAFS measurements clarify the chemical state and the molecular conformation. The XPS data provide evidence for a zwitterionic adsorption configuration at all temperatures, and NEXAFS results prove that the side chain aromatic system adsorbs with a 37° tilted geometry with respect to the substrate plane allowing parallel-displaced $\pi-\pi$ coupling between narrower rows and therefore the emergence of regularly structured 2D supramolecular domains.

We emphasize the similarity of the present self-assembly scenario with the case of L-methionine on Ag(111)[32] and on Cu(111)[40] presented in our previous studies. This is understood as a strong indication that the zwitterionic noncovalent intermolecular bonding scheme of amino acids represents a general construction motif on weakly reactive close-packed metal surfaces that consequently should follow a universal trend driven by zwitterionicity and hydrogen-bonding between the carboxylate and ammonium functional groups. The difference between the two systems regarding their mesoscopic ordering is a consequence of the conformational surface adaptation and chemical reactivity of the side chains.

It is important to point out that this study on the organization of L-tyrosine on Ag(111), whose 1D character and zwitterionic dimerization mechanism was adumbrated by our previous works,[32,40] contributes to a systematic development toward the control of supramolecular interactions, that is progressing from trial-and-error-type experiments to more predictable and systematic exploitation of specific functionalities and molecular recognition schemes. Here, the molecular dimerization and linear extension of the 2D confined molecular assembly is the direct consequence of the amino acid ammonium and carboxylate moieties, whereas the mesoscopic organization can be achieved by specific side chain engineering. Accordingly, the basic understanding of nanopatterning with amino acids and bonding of biomolecules at surfaces might yield a general pathway for noncovalent synthesis of low-dimensional architectures with controlled morphology and functionality at the nanoscale.

MATERIALS AND METHODS

Sample Preparation. All experiments were carried out in UHV at a base pressure of 2×10^{-10} mbar. The L-tyrosine molecules (Sigma-Aldrich, purity >99.0%) were deposited onto the noble-metal surfaces by organic molecular beam epitaxy. The amino acid powder was evaporated by resistive heating at 370 K from a quartz crucible. Prior to the amino acid adsorption, the monocrystalline Ag(111) and Cu(111) substrates were cleaned by successive cycles of Ar^+ sputtering at 4 μA and 1 keV, and annealing at 770 K. During the molecular deposition, the substrate was held at temperatures between 170 and 320 K.

Scanning Tunneling Microscopy. After surface preparation and molecular deposition the sample was cooled down below 15 K for *in situ* STM. The STM measurements were performed in a custom-designed UHV chamber[60] equipped with a commercial state-of-the-art Besocke-type low-temperature STM.[61] All the presented topographical STM images were obtained by the constant-current method. All displayed STM figures were treated with the WSXM software.[62]

X-ray Photoelectron Spectroscopy and Near-Edge X-ray Absorption Fine Structure. The X-ray experiments were performed at the ALOISA beamline of the ELETTRA synchrotron. The X-ray beam is characterized by an intensity of 4×10^{10} photon/(s · mm^2) and an elliptical photon polarization factor of 0.95.[63] Because of this high polarization factor, we regard the beam as perfectly linearly polarized. The samples were prepared *in situ* under the same conditions as for the STM section. The XPS measurements were performed for submonolayer and saturated monolayer preparations, the spectra showing no molecular coverage dependence,

whereas for NEXAFS only the saturated monolayer case was considered. During the X-ray measurements, the sample was held at a temperature of ~200 K to minimize X-ray induced artifacts.[64] The XPS spectra were obtained with a photon beam energy of 600 eV and an incident beam grazing angle of 3°. The absolute binding energy was calibrated by tuning the spectra with the substrate Ag 3d peaks. The acquired experimental data was fitted with Voigt functions and a Shirley-type background. The NEXAFS data were acquired with an incident grazing angle of 7° and were normalized by dividing the saturated monolayer partial yield signal with the one of the clean substrate. The PEY for the NEXAFS measurements was collected by a wide acceptance angle channeltron with a high energy pass filter set to 250 eV. The high photon polarizability permits studying the polarization dependence of the NEXAFS spectra and therefore gaining intramolecular conformational information. The sample can be rotated around the axis defined by the intersection of the incidence and substrate planes, hence the X-ray absorption dependence with respect to photon polarization is considered for the same photon incident angle. The absolute photon energy was calibrated by identifying in the absorption spectra the C 1s $\rightarrow \pi^*$ resonance of gas phase CO in the ALOISA ionization cell.[63] The NEXAFS spectra were fitted following the building block principle[42] with Gaussian functions and an error function to take account of the IP edge.

Acknowledgment. This work was financially supported by NSERC, CFI, DFG, SNF, and the DAAD.

Supporting Information Available: STM topographs of the L-tyrosine self-assembled β domains on Ag(111) showing a measurement-induced structural reconfiguration; STM topograph of L-tyrosine adsorbed on Cu(111) at a surface temperature of 290 K, demonstrating substrate-mediated molecular fragmentation; N 1s XPS spectrum for the low temperature saturated monolayer phase; table of the fitting parameters for the Gaussian curves of the C 1s NEXAFS spectra; interaction energy maps of a two-molecule system calculated with the MM+ force-field. This material is available free of charge *via* the Internet at http://pubs.acs.org.

REFERENCES AND NOTES

1. Mann, S. Life as a Nanoscale Phenomenon. *Angew. Chem., Int. Ed.* **2008**, *47*, 5306–5320.
2. Klug, A. From Macromolecules to Biological Assemblies (Nobel Lecture). *Angew. Chem., Int. Ed.* **1983**, *22*, 565–582.
3. Kushner, D. J. Self-Assembly of Biological Structures. *Bacteriol Rev.* **1969**, *33*, 302–345.
4. Myers, J. K.; Pace, C. N. Hydrogen Bonding Stabilizes Globular Proteins. *Biophys. J.* **1996**, *71*, 2033–2039.
5. McGaughey, G. B.; Gagne, M.; Rappe, A. K. π-Stacking Interactions—Alive and Well in Proteins. *J. Biol. Chem.* **1998**, *273*, 15458–15463.
6. Butterfield, S. M.; Patel, P. R.; Waters, M. L. Contribution of Aromatic Interactions to Alpha-Helix Stability. *J. Am. Chem. Soc.* **2002**, *124*, 9751–9755.
7. Burley, S. K.; Petsko, G. A. Aromatic−Aromatic Interaction—A Mechanism of Protein-Structure Stabilization. *Science* **1985**, *229*, 23–28.
8. Serrano, L.; Bycroft, M.; Fersht, A. R. Aromatic Aromatic Interactions and Protein Stability—Investigation by Double-Mutant Cycles. *J. Mol. Biol.* **1991**, *218*, 465–475.
9. Furukawa, M.; Tanaka, H.; Sugiura, K.; Sakata, Y.; Kawai, T. Fabrication of Molecular Alignment at the Specific Sites on Cu(111) Surfaces Using Self-Assembly Phenomena. *Surf. Sci.* **2000**, *445*, L58–L63.
10. Kawai, T.; Tanaka, H.; Nakagawa, T. Low Dimensional Self-Organization of DNA-Base Molecules on Cu(111) Surfaces. *Surf. Sci.* **1997**, *386*, 124–136.
11. Chen, Q.; Richardson, N. V. Enantiomeric Interactions between Nucleic Acid Bases and Amino Acids on Solid Surfaces. *Nat. Mater.* **2003**, *2*, 324–328.
12. Tomba, G.; Lingenfelder, M.; Costantini, G.; Kern, K.; Klappenberger, F.; Barth, J. V.; Ciacchi, L. C.; De Vita, A. Structure and Energetics of Diphenylalanine Self-Assembling on Cu(110). *J. Phys. Chem. A* **2007**, *111*, 12740–12748.
13. Kelly, R. E. A.; Kantorovich, L. N. Planar Nucleic Acid Base Super-Structures. *J. Mater. Chem.* **2006**, *16*, 1894–1905.
14. Otero, R.; Schock, M.; Molina, L. M.; Laegsgaard, E.; Stensgaard, I.; Hammer, B.; Besenbacher, F. Guanine Quartet Networks Stabilized by Cooperative Hydrogen Bonds. *Angew. Chem., Int. Ed.* **2005**, *44*, 2270–2275.
15. Forster, M.; Dyer, M. S.; Persson, M.; Raval, R. Probing Conformers and Adsorption Footprints at the Single-Molecule Level in a Highly Organized Amino Acid Assembly of (S)-Proline on Cu(110). *J. Am. Chem. Soc.* **2009**, *131*, 10173–10181.
16. Yokoyama, T.; Yokoyama, S.; Kamikado, T.; Mashiko, S. Nonplanar Adsorption and Orientational Ordering of Porphyrin Molecules on Au(111). *J. Chem. Phys.* **2001**, *115*, 3814–3818.
17. Jung, T. A.; Schlittler, R. R.; Gimzewski, J. K. Conformational Identification of Individual Adsorbed Molecules with the STM. *Nature* **1997**, *386*, 696–698.
18. Auwarter, W.; Klappenberger, F.; Weber-Bargioni, A.; Schiffrin, A.; Strunskus, T.; Woll, C.; Pennec, Y.; Riemann, A.; Barth, J. V. Conformational Adaptation and Selective Adatom Capturing of Tetrapyridyl-Porphyrin Molecules on a Copper (111) Surface. *J. Am. Chem. Soc.* **2007**, *129*, 11279–11285.
19. Kasemo, B. Biological Surface Science. *Surf. Sci.* **2002**, *500*, 656–677.
20. Barth, J. V.; Costantini, G.; Kern, K. Engineering Atomic and Molecular Nanostructures on Surfaces. *Nature* **2005**, *437*, 671–679.
21. Barth, J. V. Molecular Architectonic on Metal Surfaces. *Annu. Rev. Phys. Chem.* **2007**, *58*, 375–407.
22. Elemans, J. A. A. W.; Lei, S. B.; De Feyter, S. Molecular and Supramolecular Networks on Surfaces: From Two-Dimensional Crystal Engineering to Reactivity. *Angew. Chem., Int. Ed.* **2009**, *48*, 7298–7332.
23. Barlow, S. M.; Raval, R. Complex Organic Molecules at Metal Surfaces: Bonding, Organisation and Chirality. *Surf. Sci. Rep.* **2003**, *50*, 201–341.
24. Kühnle, A.; Linderoth, T. R.; Hammer, B.; Besenbacher, F. Chiral Recognition in Dimerization of Adsorbed Cysteine Observed by Scanning Tunneling Microscopy. *Nature* **2002**, *415*, 891–893.
25. Rosei, F.; Schunack, M.; Naitoh, Y.; Jiang, P.; Gourdon, A.; Laegsgaard, E.; Stensgaard, I.; Joachim, C.; Besenbacher, F. Properties of Large Organic Molecules at Surfaces. *Prog. Surf. Sci.* **2003**, *71*, 95–146.
26. Pennec, Y.; Auwarter, W.; Schiffrin, A.; Weber-Bargioni, A.; Riemann, A.; Barth, J. V. Supramolecular Gratings for Tuneable Confinement of Electrons on Metal Surfaces. *Nat. Nanotechnol.* **2007**, *2*, 99–103.
27. Schiffrin, A.; Reichert, J.; Auwarter, W.; Jahnz, G.; Pennec, Y.; Weber-Bargioni, A.; Stepanyuk, V. S.; Niebergall, L.; Bruno, P.; Barth, J. V. Self-Aligning Atomic Strings in Surface-Supported Biomolecular Gratings. *Phys. Rev. B* 2008, 78.
28. Preuss, M.; Schmidt, W. G.; Bechstedt, F. Coulombic Amino Group-Metal Bonding: Adsorption of Adenine on Cu(110). *Phys. Rev. Lett.* **2005**, *94*, 236102.
29. Nyberg, M.; Hasselstrom, J.; Karis, O.; Wassdahl, N.; Weinelt, M.; Nilsson, A.; Pettersson, L. G. M. The Electronic Structure and Surface Chemistry of Glycine Adsorbed on Cu(110). *J. Chem. Phys.* **2000**, *112*, 5420–5427.
30. Liu, L. L.; Franz, K. J. Phosphorylation-Dependent Metal Binding by Alpha-Synuclein Peptide Fragments. *J. Biol. Inorg. Chem.* **2007**, *12*, 234–247.
31. Wang, D.; Xu, Q. M.; Wan, L. J.; Bai, C. L.; Jin, G. Adsorption of Enantiomeric and Racemic Tyrosine on Cu(111): A Scanning Tunneling Microscopy Study. *Langmuir* **2003**, *19*, 1958–1962.
32. Schiffrin, A.; Riemann, A.; Auwarter, W.; Pennec, Y.; Weber-Bargioni, A.; Cvetko, D.; Cossaro, A.; Alberto, M.; Barth, J. V.

Zwitterionic Self-Assembly of L-Methionine Nanogratings on the Ag(111) Surface. *Proc. Natl. Acad. Sci. U.S.A.* **2007**, *104*, 5279–5284.
33. Zubavichus, Y.; Zharnikov, M.; Shaporenko, A.; Fuchs, O.; Weinhardt, L.; Heske, C.; Umbach, E.; Denlinger, J. D.; Grunze, M. Soft X-ray Induced Decomposition of Phenylalanine and Tyrosine: A Comparative Study. *J. Phys. Chem. A* **2004**, *108*, 4557–4565.
34. Zubavichus, Y.; Fuchs, O.; Weinhardt, L.; Heske, C.; Umbach, E.; Denlinger, J. D.; Grunze, M. Soft X-Ray-Induced Decomposition of Amino Acids: An XPS, Mass Spectrometry, and NEXAFS Study. *Radiat. Res.* **2004**, *161*, 346–358.
35. Boese, J.; Osanna, A.; Jacobsen, C.; Kirz, J. Carbon Edge Xanes Spectroscopy of Amino Acids and Peptides. *J Electron Spectrosc.* **1997**, *85*, 9–15.
36. Kaznacheyev, K.; Osanna, A.; Jacobsen, C.; Plashkevych, O.; Vahtras, O.; Agren, H. A.; Carravetta, V.; Hitchcock, A. P. Innershell Absorption Spectroscopy of Amino Acids. *J. Phys. Chem. A* **2002**, *106*, 3153–3168.
37. Gonella, G.; Terreni, S.; Cvetko, D.; Cossaro, A.; Mattera, L.; Cavalleri, O.; Rolandi, R.; Morgante, A.; Floreano, L.;M., C. Ultrahigh Vacuum Deposition of L-Cysteine on Au(110) Studied by High-Resolution X-ray Photoemission: From Early Stages of Adsorption to Molecular Organization. *J. Phys. Chem. B* **2005**, *109*, 18003–18009.
38. Hasselstrom, J.; Karis, O.; Weinelt, M.; Wassdahl, N.; Nilsson, A.; Nyberg, M.; Pettersson, L. G. M.; Samant, M. G.; Stohr, J. The Adsorption Structure of Glycine Adsorbed on Cu(110); Comparison with Formate and Acetate/Cu(110). *Surf. Sci.* **1998**, *407*, 221–236.
39. Riemann, A.; Nelson, B. Molecular Wires Self-Assembled on a Graphite Surface. *Langmuir* **2009**, *25*, 4522–4525.
40. Schiffrin, A.; Reichert, J.; Pennec, Y.; Auwarter, W.; Weber-Bargioni, A.; Marschall, M.; Dell'Angela, M.; Cvetko, D.; Bavdek, G.; Cossaro, A.; *et al*. Self-Assembly of L-Methionine on Cu(111): Steering Chiral Organization by Substrate Reactivity and Thermal Activation. *J. Phys. Chem. C* **2009**, *113*, 12101–12108.
41. Frey, M. N.; Koetzle, T. F.; Lehmann, M. S.; Hamilton, W. C. Precision Neutron-Diffraction Structure Determination of Protein and Nucleic-Acid Components. 10. Comparison between Crystal and Molecular-Structures of L-Tyrosine and L-Tyrosine Hydrochloride. *J. Chem. Phys.* **1973**, *58*, 2547–2556.
42. Stohr, J. *NEXAFS Spectroscopy*, 1st ed.; Springer: New York, 1992; Vol. 25.
43. Cossaro, A.; Terreni, S.; Cavalleri, O.; Prato, M.; Cvetko, D.; Morgante, A.; Floreano, L.; Canepa, M. Electronic and Geometric Characterization of the L-Cysteine Paired-Row Phase on Au(110). *Langmuir* **2006**, *22*, 11193–11198.
44. Zubavichus, Y.; Shaporenko, A.; Grunze, M.; Zharnikov, M. Innershell Absorption Spectroscopy of Amino Acids at All Relevant Absorption Edges. *J. Phys. Chem. A* **2005**, *109*, 6998–7000.
45. Zhang, W. H.; Carravetta, V.; Plekan, O.; Feyer, V.; Richter, R.; Coreno, M.; Prince, K. C. Electronic Structure of Aromatic Amino Acids Studied by Soft X-ray Spectroscopy. *J. Chem. Phys.* **2009**, *131*, 035103.
46. Puttner, R.; Kolczewski, C.; Martins, M.; Schlachter, A. S.; Snell, G.; Sant'Anna, M.; Viefhaus, J.; Hermann, K.; Kaindl, G. The C 1s NEXAFS Spectrum of Benzene below Threshold: Rydberg or Valence Character of the Unoccupied σ-Type Orbitals. *Chem. Phys. Lett.* **2004**, *393*, 361–366.
47. Ghiringhelli, L. M.; Delle Site, L. Phenylalanine near Inorganic Surfaces: Conformational Statistics *vs* Specific Chemistry. *J. Am. Chem. Soc.* **2008**, *130*, 2634–2638.
48. Allinger, N. L. Conformational Analysis. 130. MM2. Hydrocarbon Force-Field Utilizing V_1 and V_2 Torsional Terms. *J. Am. Chem. Soc.* **1977**, *99*, 8127–8134.
49. Lii, J. H.; Gallion, S.; Bender, C.; Wikstrom, H.; Allinger, N. L.; Flurchick, K. M.; Teeter, M. M. Molecular Mechanics (MM2) Calculations on Peptides and on the Protein Crambin Using the Cyber-205. *J. Comput. Chem.* **1989**, *10*, 503–513.
50. Paton, R. S.; Goodman, J. M. Hydrogen Bonding and π-Stacking: How Reliable Are Force Fields? A Critical Evaluation of Force Field Descriptions of Nonbonded Interactions. *J. Chem. Inf. Model.* **2009**, *49*, 944–955.
51. Hunter, C. A.; Sanders, J. K. M. The Nature of π−π Interactions. *J. Am. Chem. Soc.* **1990**, *112*, 5525–5534.
52. Tsuzuki, S.; Honda, K.; Uchimaru, T.; Mikami, M.; Tanabe, K. Origin of Attraction and Directionality of the X/X Interaction: Model Chemistry Calculations of Benzene Dimer Interaction. *J. Am. Chem. Soc.* **2002**, *124*, 104–112.
53. Sinnokrot, M. O.; Sherrill, C. D. High-Accuracy Quantum Mechanical Studies of π−π Interactions in Benzene Dimers. *J. Phys. Chem. A* **2006**, *110*, 10656–10668.
54. Seo, J. I.; Kim, I.; Lee, Y. S. π−π Interaction Energies in Monosubstituted-Benzene Dimers in Parallel- and Antiparallel-Displaced Conformations. *Chem. Phys. Lett.* **2009**, *474*, 101–106.
55. Grimme, S. Do Special Noncovalent π−π Stacking Interactions Really Exist. *Angew. Chem., Int. Ed.* **2008**, *47*, 3430–3434.
56. Gutzler, R.; Lappe, S.; Mahata, K.; Schmittel, M.; Heckl, W. M.; Lackinger, M. Aromatic Interaction *vs* Hydrogen Bonding in Self-Assembly at the Liquid−Solid Interface. *Chem. Commun.* **2009**, 680–682.
57. Schneider, H. J. Binding Mechanisms in Supramolecular Complexes. *Angew. Chem., Int. Ed.* **2009**, *48*, 3924–3977.
58. Klappenberger, F.; Canas-Ventura, M. E.; Clair, S.; Pons, S.; Schlickum, U.; Qu, Z. R.; Brune, H.; Kern, K.; Strunskus, T.; Woll, C.; *et al*. Conformational Adaptation in Supramolecular Assembly on Surfaces. *Chemphyschem.* **2007**, *8*, 1782–1786.
59. Klappenberger, F.; Canas-Ventura, M. E.; Clair, S.; Pons, S.; Schlickum, U.; Qu, Z. R.; Strunskus, T.; Comisso, A.; Woll, C.; Brune, H.; *et al*. Does the Surface Matter? Hydrogen-Bonded Chain Formation of an Oxalic Amide Derivative in a Two- and Three-Dimensional Environment. *Chemphyschem.* **2008**, *9*, 2522–2530.
60. Auwarter, W.; Schiffrin, A.; Weber-Bargioni, A.; Pennec, Y.; Riemann, A.; Barth, J. V. Molecular Nanoscience and Engineering on Surfaces. *Int. J. Nanotechnol.* **2008**, *5*, 1171–1193.
61. Meyer, G. A Simple Low Temperature Ultra-High Vacuum Scanning Tunneling Microscope Capable of Atomic Manipulation. *Rev. Sci. Instrum.* **1996**, *67*, 2960.
62. Horcas, I.; Fernandez, R.; Gomez-Rodriguez, J. M.; Colchero, J.; Gomez-Herrero, J.; Baro, A. M. WSXM: A Software for Scanning Probe Microscopy and a Tool for Nanotechnology. *Rev. Sci. Instrum.* **2007**, *78*, 013705.
63. Floreano, L.; Naletto, G.; Cvetko, D. R, G.; Malvezzi, M.; Marassi, L.; Morgante, A.; Santaniello, A.; Verdini, A.; Tommasini, F.; Tondello, G. Performance of the Grating-Crystal Monochromator of the ALOISA Beamline at the ELETTRA Synchrotron. *Rev. Sci. Instrum.* **1999**, *70*, 3855.
64. Feulner, P.; Niedermayer, T.; Eberle, K.; Schneider, R.; Menzel, D.; Baumer, A.; Schmich, E.; Shaporenko, A.; Tai, Y.; Zharnikov, M. Strong Temperature Dependence of Irradiation Effects in Organic Layers. *Phys. Rev. Lett.* **2004**, *93*, 178302.